Research Article Vol. 61, No. 1 / 1 January 2022 / Applied Optics 287

applied optics

High precision angular displacement measurement based on self-correcting error compensation of three image sensors

Hai Yu,* Qiuhua Wan, Xinran Lu, Changhai Zhao, and Lihui Liang

Changchun Institute of Optics, Fine Mechanics and Physics, Chinese Academy of Sciences, Changchun 130033, China
**Corresponding author: yuhai@ciomp.ac.cn*

Received 26 October 2021; revised 2 December 2021; accepted 7 December 2021; posted 10 December 2021; published 22 December 2021

As the feedback link of a numerical control system, the measurement accuracy of absolute angular displacement measurements directly affects the control performance of a numerical control system. In previous research, angular displacement measurements based on dual image sensors can achieve higher measurement performance. However, the elimination of harmonic error by the dual image sensor is still limited. For this reason, this paper proposes an image-type angular displacement measurement method based on self-correction error compensation of three image sensors. First, the mathematical model of harmonic error is established, and the shortcomings of using dual image sensors to compensate the error are analyzed. Then, a high precision angular displacement measurement method based on three image sensors is proposed. Finally, the self-correction error compensation method of three image sensors is applied to the angular displacement measurement system, and the measurement performance is verified. The experimental results show that a measurement accuracy of 1.76″ can be achieved on the circular grating with a diameter of 96 mm. In contrast, the dual image sensor can only achieve a measurement accuracy of 2.88″. It is concluded that the odd number of image sensors can achieve higher measurement accuracy than the even number. This research lays a foundation for the realization of high precision image angular displacement measurement.

https://doi.org/10.1364/AO.446859

1. INTRODUCTION

The development of precise displacement measurement technology is directly related to the control level of data equipment [1,2]. To date, the most commonly used displacement measurement strategies include optical grating measurements [3,4], capacitive grating measurements [5,6], and magnetic grating measurements [7,8]. Similar to grating displacement measurement, angular displacement measurement (ADM) technology based on image recognition algorithm is a new kind of measurement technology [6,9,10]. Advantages of digital image processing technology are high flexibility, robustness, and fault tolerance, and it cannot be affected by the amplitude difference, phase offset, period correction, or other factors of traditional moiré fringe ADM. With this method, it is easier to achieve high resolution and high precision measurements. At the same time, due to the use of "all digital signal" processing methods, digital operation can be added in the process of signal acquisition, so as to improve the measurement performance [11–13]. Therefore, image-type ADM is an important research direction for new measurement technologies in the future.

In 2003, while researching image-type ADM, Leviton [14] used an area scan CCD to receive grating patterns with reference lines and binary symbols, achieving a measurement resolution of 0.01" and an accuracy of 0.2 μm. Sugiyam [15] studied absolute displacement measurement technology based on area scan detectors in 2008 and realized 14-bit angular resolution on a circular grating with a diameter of 30 mm. In 2015, Kim [16] realized 13-bit encoding recognition on a 41.72 mm diameter grating with a measurement accuracy of 0.044° by using phase-shift encoding and a micro-image detection system. Mu [17] used CMOS image sensors to identify pseudo-random single channel coding in 2019 and realized up to 20-bit coding recognition. Yuan [18] proposed a robust high precision subdivision algorithm in 2019, which realized 1.6″ ADM accuracy on a grating with an outer diameter of 79 mm.

According to previous research and analysis, the results of ADM contain multiple harmonic errors. To reduce these measurement errors, Tan [19] proposed a method of online correction of measurement signals by using a radial basis function, Lu [20] proposed an automatic correction time measurement dynamic reverse (TDR) method for ADMs, Watanabe [21] proposed an error calibration method with five reading heads evenly distributed around the circumference, and Probst [22] proposed an error compensation method based on eight reading heads. According to this research literature, in the traditional research (mostly based on the moiré fringe measurement method), when

multiple reading heads are used for measurement, the moiré fringe signal synthesized by multiple reading heads needs to be adjusted. However, for the image displacement measurement technology, due to the full digital displacement measurement method, there is no synthetic waveform of the analog signal.

Therefore, the reason of multi-reading head measurement in image measurement needs to be studied. In previous research, we proposed a self-correction error compensation algorithm based on dual image sensors and achieved a measurement accuracy of 6.33″ on a grating with an outer diameter of 38 mm [23]. However, the error compensation effect of dual image sensors is not obvious for even harmonic errors in image-type ADM. To further improve the accuracy of image-type ADM, this paper proposes a self-correction error compensation method using three image sensors to further improve the measurement accuracy.

The layout of this paper is as follows: Section 2 introduces the principle of image-type ADM, Section 3 analyzes the error harmonic component in ADM, Section 4 proposes the error self-correction compensation algorithm using three image sensors, Section 5 is the experimental verification, and Section 6 is the summary.

2. PRINCIPLE OF IMAGE ANGULAR DISPLACEMENT MEASUREMENT

Image-type ADM uses a digital image recognition algorithm to measure the displacement of the calibration grating. The image sensor is used to collect the pattern on the calibration grating, and then the displacement measurement is realized through the digital image recognition algorithm. The measurement principle is shown in Fig. 1.

In previous research [24], M-sequence pseudo-random coding is used to design the single loop absolute coding grating, and the "wide" and "narrow" coding lines are set in the calibration grating, which represent the "1" and "0" coding elements, respectively, as shown in the coding pattern in Fig. 1. Suppose that the circle of the calibration grating contains 2^n coding lines. By identifying n "wide" and "narrow" coding lines, the current coding value in the image field can be obtained. By decoding the coding value, the current absolute position can be obtained, expressed as θ_c.

At the same time, to further improve the measurement resolution, an angular displacement subdivision algorithm has been proposed in the early stages [11,12], and further subdivision operation is performed between the two coded lines. The principle of the subdivision algorithm is shown in Fig. 2.

In Fig. 2, the center point of the image sensor is set at point C, $L1$ and $L2$ are the two coding lines on both sides of point C, and the linear image sensor intersects with $L1$ and $L2$ at points A and B, respectively. If the angle between $L1$ and $L2$ in circular grating is η, then the subdivision operation is shown in Eq. (1),

$$\theta_s = \eta \cdot \frac{BC}{AB}. \tag{1}$$

In Eq. (1), BC and AB are lengths that the image sensor can obtain. To realize a quantitative value of the subdivision value, let $\eta = 2^m$, so that the angular displacement subdivision operation of 2^m times is realized. For the positions of points A and B in Fig. 2, the centroid algorithm will be used for calculations. Finally, the binary value of image-type ADM output will be composed of decoded value θ_c and subdivision value θ_s, that is, the measured value $\theta = 2^m\theta_c + \theta_s$.

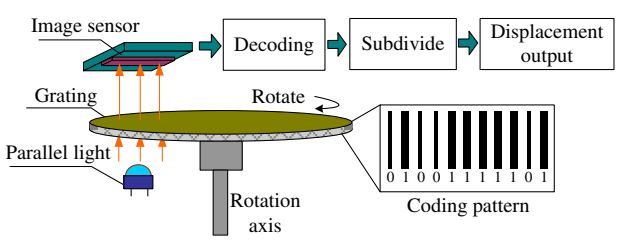

Fig. 1. Schematic diagram of image-type ADM.

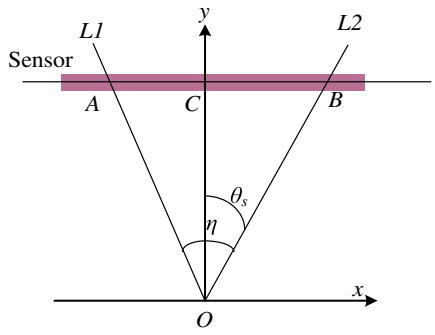

Fig. 2. Schematic of the subdivision algorithm.

3. HARMONIC ERROR ANALYSIS

According to the previous research, the main method to eliminate ADM is to increase the number of reading heads, that is, install p reading heads evenly in the circumference of the grating code disk and take the average value of p reading values as the measured value. Different from the moiré fringe measurement method, the error compensation algorithm for multi-reading head in the image-type ADM is different from that in traditional research. The influence of the multi-reading head measurement method on the error needs to be reanalyzed. In the image-type ADM technology, when there are p reading heads in the circumference, the situation is shown in Fig. 3.

A. Establishment of the Harmonic Error Model

When there is only a single image sensor ($p = 1$) used in image-type ADM, the measured value θ includes the true angle value θ_r and the error value $e(\theta)$, as shown in Eq. (2),

$$\theta = \theta_r + e(\theta). \tag{2}$$

According to the composition of measurement error, the error $e(\theta)$ contains multiple times harmonic components. The error $e(\theta)$ can be expressed in the form of a Fourier series, as shown in Eq. (3) [25],

$$e(\theta) = \sum_{k=1}^{\infty} w_k \sin(k\theta), \tag{3}$$

where k is the harmonic number and w_k is the amplitude of the kth harmonic.

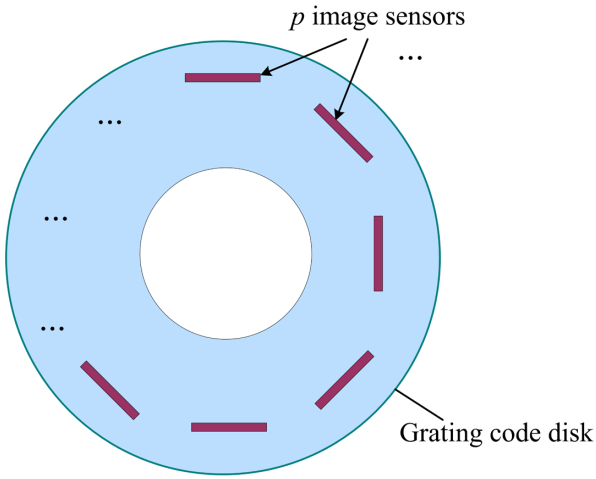

Fig. 3. p image sensors are uniformly distributed around the circumference of the grating.

To eliminate the harmonic error, p image sensors (reading heads) were used and evenly distributed on the circumference of the calibration grating. The respective measured values of the p image sensors are taken as the mean value, as shown in Eq. (4),

$$\begin{aligned} E(\theta) &= \frac{1}{p}\left\{e(\theta) + e\left(\theta + \frac{2\pi}{p}\right) + \ldots + e\left[\theta + (p-1)\cdot\frac{2\pi}{p}\right]\right\} \\ &= \frac{1}{p}\sum_{k=1}^{\infty} w_k \left\{\sin k\theta + \sin k\left(\theta + \frac{2\pi}{p}\right)\right. \\ &\quad + \sin k\left(\theta + 2\cdot\frac{2\pi}{p}\right) + \ldots \\ &\quad \left. + \sin k\left[\theta + (p-1)\cdot\frac{2\pi}{p}\right]\right\} \\ &= \sum_{k}^{\infty} E_k(\theta), \end{aligned} \tag{4}$$

where $E_k(\theta)$ is the error component of the kth harmonic after taking the mean value of p image sensors. For different time harmonic errors, the average value of the kth can be expressed as follows:

$$E_k(\theta) = \begin{cases} w_k \sin k\theta, & k = cp,\ c = 1, 2, 3, \ldots \\ 0, & k \neq cp,\ c = 1, 2, 3, \ldots \end{cases}, \tag{5}$$

where c is a nonzero integer. It can be seen that only $k = cp(c = 1,\ 2,\ 3,\ \ldots)$ are retained in Eq. (5). Therefore, when p image sensors (reading heads) are used in ADM, only the harmonic errors with integral multiples of p are retained in the resultant error $E_k(\theta)$.

B. Analysis on the Number of Reading Heads

In traditional technology, double image sensors (reading heads) are often used to eliminate errors. However, when using dual image sensors (reading heads), the elimination of errors has limitations. The analysis is as follows:

According to the mathematical model of error, the two main errors that affect the measurement of angular displacement are the grating eccentricity error and subdivision operation error. Since the circular grating contains 2^n periodic coding lines, the error variation frequency in each line cycle is an integer multiple of 2^n. So the mathematical model of error in Eq. (3) can be approximately to the sum of the one-time harmonic error and multiple 2^n times harmonic errors, as shown in Eq. (6),

$$e(\theta) \approx \sum_{k=1}^{\infty} w_k[\sin\theta + \sin(2^n\theta)\ldots], \tag{6}$$

where 2^n is the number of coded lines in the circular grating. The first term $\sin\theta$ on the right side of the equation represents the one-time harmonic caused by the eccentricity of the circular grating, and the harmonic errors such as $\sin(2^n\cdot\theta)$ are caused by subdivision operation [as shown in Eq. (1)]. It can be seen that in addition to the one-time harmonic caused by eccentricity, the error is mainly affected by even harmonic errors.

The influence of the one-time harmonic error can be eliminated when using a dual image sensor ($p = 2$) in ADM. However, according to the analysis of Eq. (2), the even harmonic error component in the measurement result cannot be removed by a dual image sensor.

Based on the appeal analysis, it can be concluded that:

(a) More reading heads can eliminate more harmonic errors;
(b) Odd reading heads are easier to improve the measurement accuracy than even reading heads.

Therefore, using an odd number of sensors to achieve error correction can eliminate the more error component in ADM. So, we propose to use odd image sensors to eliminate the error. Limited by the space of the measuring device, we will use three image sensors instead of two image sensors.

4. SYNTHETIC MEASUREMENT ALGORITHM OF THREE IMAGE SENSORS

Because of the full digital signal processing, an image-type ADM can realize the error compensation algorithm more flexibly. Different from traditional moiré fringe technology, the image-type ADM needs to calculate the compensation value by the digital algorithm. In image-type ADM, because the subdivision algorithm of Eq. (1) is adopted, directly averaging the values measured by three reading heads cannot eliminate the error to the greatest extent. In addition, image-type ADM needs to first calculate the subdivision lengths BC and AB. Therefore, it is necessary to synthesize the subdivision lengths BC and AB.

When three image sensors (reading heads) are used, the arrangement of the three reading heads is shown in Fig. 4(a).

In Fig. 4(a), #1, #2, and #3 are three image sensors, and the angle between them is $\beta = 2\pi/3$. In the ideal state, the intersection points between the #1 image sensor and the coding lines are A and B. Set point C be the center of the image, which does not change with the movement of the grating. At this time, the distance of the coding lines detected by the #1 image sensor is AB. Similarly, for the #2 and #3 image sensors, the distances of the coding lines are equal to AB. In addition, the distance OC

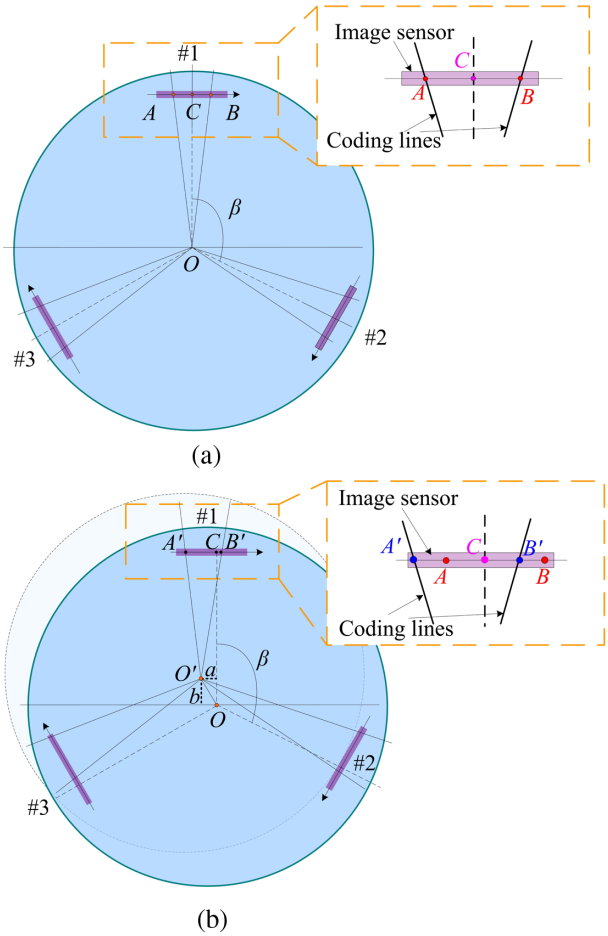

Fig. 4. Measurement principle of three image sensors. (a) In the ideal state and (b) when there is eccentricity.

between the #1 image sensor center C and the rotating spindle center O is the same as the #2 and #3 image sensors.

When there is eccentricity, the center of the calibration grating will deviate from the center of rotation [as shown in Fig. 4(b)]. The calibration grating center O' deviates from the rotation axis center O. The offset generated in the transverse direction is a, and the offset in the longitudinal direction is b. The length BC collected by the image sensor becomes $B'C'$, and AB becomes $A'B'$. Then, the two length values obtained during the subdivision operation in #1 image sensor are

$$A'B'|_{\#1} = \frac{OC - b}{OC} AB, \tag{7}$$

$$B'C'|_{\#1} = \frac{OC - b}{OC} BC - a, \tag{8}$$

where AB and BC are the lengths collected from the #1 sensor in the ideal state, and $A'B'$ and $B'C'$ are the lengths after the change in Fig. 4(b).

According to the coordinate transformation, when there is eccentricity in Fig. 4(b), the two lengths obtained by #2 image sensor are as follows:

$$A'B'|_{\#2} = \frac{OC - (b\cos\beta - a\sin\beta)}{OC} AB, \tag{9}$$

$$B'C'|_{\#2} = \frac{OC - (b\cos\beta - a\sin\beta)}{OC} BC - (a\cos\beta - b\sin\beta) + \Delta_2. \tag{10}$$

In Eq. (10), Δ_2 represents the deviation of measurement value between #2 sensor and #1 sensor, and Δ_2 is a constant value.

Similarly, for the #3 image sensor, the collected lengths are

$$A'B'|_{\#3} = \frac{OC - (b\cos\beta + a\sin\beta)}{OC} AB, \tag{11}$$

$$B'C'|_{\#3} = \frac{OC - (b\cos\beta + a\sin\beta)}{OC} BC - (a\cos\beta + b\sin\beta) + \Delta_3. \tag{12}$$

In Eq. (12), Δ_3 represents the offset between the values calculated by #3 sensor and #1 sensor, and Δ_3 is also a constant value.

To remove the influence of a and b in the equation, add Eqs. (9) and (11), and also add Eqs. (10) and (12), and the results will be as follows:

$$A'B'|_{\#2} + A'B'|_{\#3} = \frac{2OC - 2b\cos\beta}{OC} AB, \tag{13}$$

$$B'C'|_{\#2} + B'C'|_{\#3} = \frac{2OC - 2b\cos\beta}{OC} BC - 2a\cos\beta + \Delta_2 + \Delta_3. \tag{14}$$

Since the angle between image sensors is $\beta = 2\pi/3$, there is $\cos\beta = -1/2$. Then Eqs. (13) and (7) can be added, and Eqs. (14) and (8) can be added too. Then, a composite variable can be obtained as follows:

$$A'B'|_{\#1} + A'B'|_{\#2} + A'B'|_{\#3} = 3AB, \tag{15}$$

$$B'C'|_{\#1} + B'C'|_{\#2} + B'C'|_{\#3} = 3BC + (\Delta_2 + \Delta_3). \tag{16}$$

Next, bring the above formula into Eq. (1), where the error compensation algorithm can be realized, as shown in Eq. (17).

$$\theta_s' = \eta \frac{B'C'|_{\#1} + B'C'|_{\#2} + B'C'|_{\#3}}{A'B'|_{\#1} + A'B'|_{\#2} + A'B'|_{\#3}} = \eta \frac{BC}{AB} + \Delta, \tag{17}$$

where $\Delta = (\Delta_2 + \Delta_3)/3AB$. By default, the value of Δ is a constant.

It can be seen that only the lengths of ideal state AB and BC are included in Eq. (17). In addition, the decoding values obtained by three image sensors are set as $\theta_c|_{\#1}$, $\theta_c|_{\#2}$, $\theta_c|_{\#3}$, respectively. Then, the decoding value after error compensation of three image sensors is as follows:

$$\theta_c' = \frac{\theta_c|_{\#1} + \theta_c|_{\#2} + \theta_c|_{\#3}}{3}. \tag{18}$$

Finally, the ADM value after error compensation is as follows:

$$\theta' = \eta \cdot \theta_c' + \theta_s', \tag{19}$$

where θ' is the measurement result of three image sensors after self-corrected error compensation.

5. EXPERIMENTS

A. Experimental Device Design

To verify the performance of the ADM with three image sensors, an experimental ADM device was designed with three image sensors, as shown in Figs. 5(a) and 5(b). The calibration grating designed in the experiment is shown in Fig. 5(c).

In Fig. 5(c), the diameter of the grating disk is 96 mm. There are $2^n = 512$ (9-bit) coding lines in the circumference of the grating. Three parallel light sources are used to irradiate the calibration grating, and the patterns on the grating are mapped to three image sensors to realize the acquisition of the 9-bit coded line.

The measuring circuit of three image sensors is shown in Fig. 6.

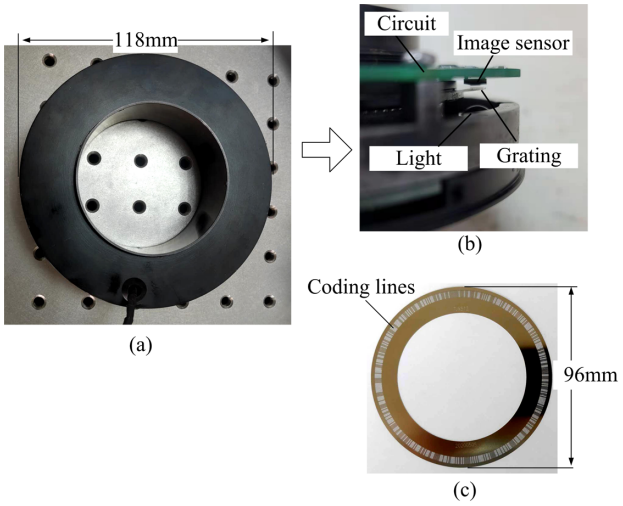

Fig. 5. Experimental device diagram. (a) Experimental device and (b) inner of the device.

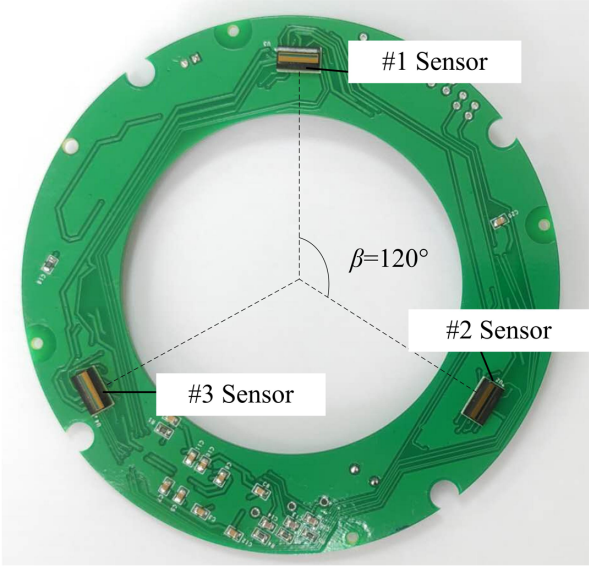

Fig. 6. Three sensor circuit.

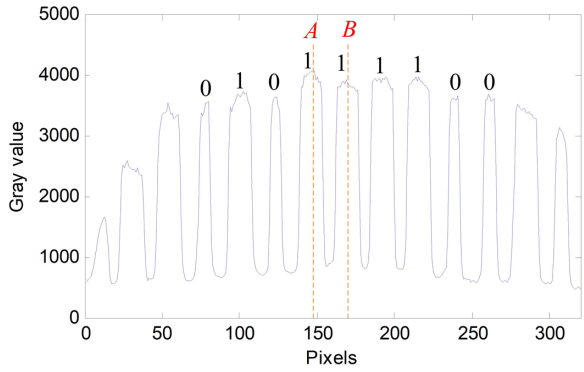

Fig. 7. Image collection.

The angle between two adjacent image sensors is $\beta = 120°$. The resolution of the image sensor is 1×320 pixels, and the pixel size is 25.4 μm. The grating pattern collected by one image sensor is shown in Fig. 7.

In Fig. 7, the effective code recognition is {0,1,0,1,1,1,1,0,0}. Through the subdivision algorithm, an angular displacement subdivision of $2^m = 2^{16}$ fold is realized between the adjacent coding lines. Finally, the designed experimental device can achieve $9 + 16 = 25$-bit ADM.

B. Precision Experiment

The accuracy of the three image sensor experimental device is tested by using the regular 17 polyhedrons. During the test, the 17 polyhedrons are coaxially installed on the rotating shaft of the experimental device, and the autocollimator is used to calibrate the errors of the 17 polyhedrons. A total of 17 points are tested, as shown in Fig. 8.

By using 17 polyhedrons, the error values are shown in Table 1. After calculation, the standard deviation of the error value in Table 1 is 1.76″.

C. Precision Comparison Experiment

To realize the precision contrast experiment, we also used the double image sensor to design the ADM circuit. At this time, double image sensor means $p = 2$. The angle between two adjacent image sensors is $\beta = 180°$, as shown in Fig. 9.

We use 17 polyhedrons to calibrate the error of the double image sensor, and the error values are shown in Table 2. After

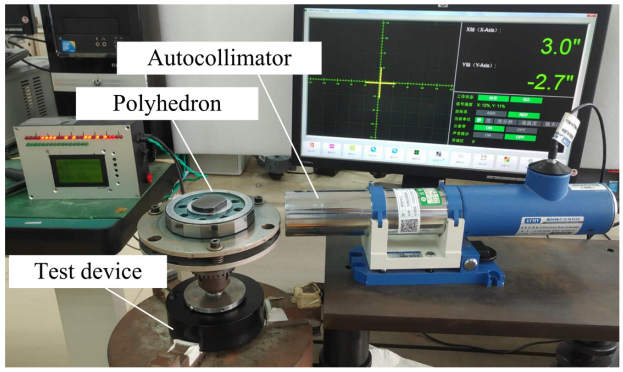

Fig. 8. Error detection test.

Table 1. Error When Using Three Sensors

No.	Errors (″)	No.	Errors (″)
1	0	10	−0.3
2	4.0	11	3.4
3	3.3	12	4.4
4	−0.9	13	1.3
5	3.4	14	2.1
6	1.4	15	3.4
7	1.8	16	0.1
8	2.3	17	3.8
9	4.4		

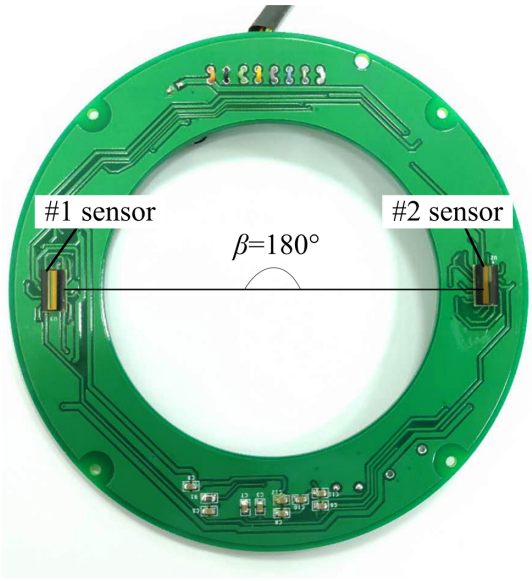

Fig. 9. Double sensor circuit for comparison.

calculation, the standard deviation of the error value in Table 2 is 2.88″.

By comparing with the error curve of three image sensors, the comparison of error curves is shown in Fig. 10.

In Fig. 10, the red curve is the error with three image sensors, and the blue curve is the error with dual image sensors. The mean square deviations of the three image sensors are $\sigma_{p=3} = 1.76''$, and the mean square deviations of the double image sensors are only $\sigma_{p=2} = 2.88''$. It can be seen that the error accuracy of three image sensors can effectively improve the measurement accuracy.

Table 2. Error When Using Double Sensors

No.	Errors (″)	No.	Errors (″)
1	0	10	−1.6
2	0.9	11	2.3
3	−4.5	12	1.3
4	2.8	13	1.4
5	3.2	14	3.4
6	−0.4	15	−4.1
7	−3.6	16	−3.2
8	−4.4	17	−4.2
9	−0.1		

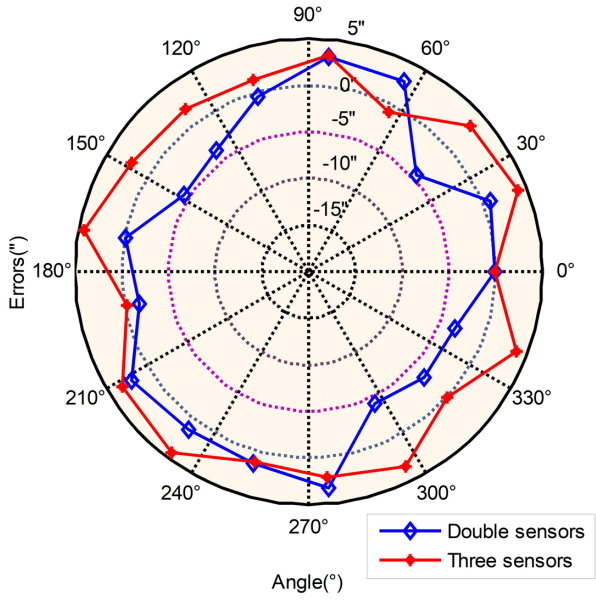

Fig. 10. Error curve.

6. CONCLUSION

Imaging-type ADM can achieve high performance measurement more easily than traditional moiré fringe, so it has become an important research content of new ADM. Based on previous research, this paper analyzes the influence of harmonic error components on the measurement results. Through the analysis, it can be concluded that (a) more reading heads can eliminate more harmonic errors and (b) odd reading heads make it easier to improve the measurement accuracy than even reading heads.

A method of high precision ADM based on three image sensors was proposed. To verify the proposed algorithm, an experimental device was designed for measurement. The diameter of the designed calibration grating was 96 mm, and the self-correction error compensation algorithm of three image sensors was used to realize the measurement accuracy of 1.76″. Compared with dual image sensors, the accuracy of the proposed method was improved from 2.88″ to 1.76″.

Compared with previous studies, our experiment achieved a measurement accuracy of 1.76″ in the miniaturized displacement measurement device. This index has great advantages in both miniaturized volume and measurement accuracy. Therefore, the experimental results show that an odd number of image sensors can more easily achieve high precision ADMs than an even number of image sensors. The research results of this paper lay a foundation for the realization of high precision ADMs.

Funding. National Natural Science Foundation of China (52075520); Jilin Scientific and Technological Development Program (20210201097GX).

Acknowledgment. We would like to thank the photoelectric displacement sensor group of the Precision Instrument and Equipment R&D Center, Changchun Institute of Optics, Fine Mechanics and Physics, Chinese Academy of Sciences.

Disclosures. The authors declare no conflicts of interest.

Data Availability. Data underlying the results presented in this paper are not publicly available at this time but may be obtained from the authors upon reasonable request.

REFERENCES

1. Z. Chen and M. Segev, "Highlighting photonics: looking into the next decade," eLight **1**, 2 (2021).
2. Z. Chen, X. Liu, K. Peng, Z. Yu, and H. Pu, "A self-adaptive interpolation method for sinusoidal sensors," IEEE Trans. Instrum. Meas. **69**, 7675–7682 (2020).
3. C.-C. Hsu, H. Chen, C.-W. Chiang, and Y.-W. Chang, "Dual displacement resolution encoder by integrating single holographic grating sensor and heterodyne interferometry," Opt. Express **25**, 30189–30202 (2017).
4. K. Hane, T. Endo, M. Ishimori, and M. Sasaki, "Integration of grating-image-type encoder using Si micromachining," Sens. Actuators A **97**, 139–146 (2002).
5. Z. Yu, K. Peng, X. Liu, Z. Chen, and Y. Huang, "A high-precision absolute angular-displacement capacitive sensor using three-stage time-grating in conjunction with a remodulation scheme," IEEE Trans. Ind. Electron. **66**, 7376–7385 (2019).
6. N. Anandan and B. George, "A wide-range capacitive sensor for linear and angular displacement measurement," IEEE Trans. Ind. Electron. **64**, 5728–5737 (2017).
7. Z. Zhang, F. Ni, Y. Dong, M. Jin, and H. Liu, "A novel absolute angular position sensor based on electromagnetism," Sens. Actuators A **194**, 196–203 (2013).
8. Z. Chen, H. Pu, X. Liu, D. Peng, and Z. Yu, "A time-grating sensor for displacement measurement with long range and nanometer accuracy," IEEE Trans. Instrum. Meas. **64**, 3105–3115 (2015).
9. J. Xue, Z. Qiu, L. Fang, Y. Lu, and W. Hu, "Angular measurement of high precision reducer for industrial robot," IEEE Trans. Instrum. Meas. **70**, 1–10 (2021).
10. F. Liu, W. Wang, L. Wang, and P. Feng, "Error analyses and calibration methods with accelerometers for optical angle encoders in rotational inertial navigation systems," Appl. Opt. **52**, 7724–7731 (2013).
11. H. Yu, Q. Wan, X. Lu, Y. Du, and S. Yang, "Small-size, high-resolution angular displacement measurement technology based on an imaging detector," Appl. Opt. **56**, 755–760 (2017).
12. H. Yu, Q. Wan, X. Lu, C. Zhao, and Y. Du, "A robust sub-pixel subdivision algorithm for image-type angular displacement measurement," Opt. Lasers Eng. **100**, 234–238 (2018).
13. H. Yu, Q. Wan, C. Zhao, X. Lu, and Y. Sun, "An anti-stain algorithm of angular displacement base on single image sensor," Appl. Opt. **59**, 1985–1990 (2020).
14. D. B. Leviton and B. J. Frey, "Ultra-high resolution, absolute position sensors for cytostatic applications," Proc. SPIE **4850**, 776–787 (2003).
15. Y. Sugiyam, Y. Matsu, H. Toyod, N. Mukozaka, and A. Ihori, "A 3.2 kHz 14-bit optical absolute rotary encoder with a CMOS profile sensor," IEEE Sens. J. **8**, 1430–1436 (2008).
16. J. A. Kim, J. W. Kim, C. S. Kang, J. Jin, and T. B. Eom, "Absolute angle measurement using a phase-encoded binary graduated disk," Measurement **80**, 288–293 (2016).
17. Y. Mu, J. Jiang, N. Ding, Q. Ni, and Y. Chang, "A 7.4 kHz, 20-bit image encoder with a CMOS linear image sensor," Opt. Quantum Electron. **51**, 321 (2019).
18. P. Yuan, D. Huang, Z. Lei, and C. Xu, "An anti-spot, high-precision subdivision algorithm for linear CCD based single-track absolute encoder," Measurement **137**, 143–154 (2019).
19. K. K. Tan and K. Z. Tang, "Adaptive online correction and interpolation of quadrature encoder signals using radial basis functions," IEEE Trans. Control Syst. Technol. **13**, 370–377 (2005).
20. X. D. Lu and D. L. Trumper, "Self-calibration of on-axis rotary encoders," CIRP Ann. **56**, 499–504 (2007).
21. T. Watanabe, M. Tadashi, and K. Makoto, "Automatic high precision calibration system for rotary encoder," J. Jpn. Soc. Precis. Eng. **67**, 1091–1095 (2001).
22. R. Probst, "Self-calibration of divided circles on the basis of a prime factor algorithm," Meas. Sci. Technol. **19**, 015101 (2008).
23. H. Yu, Q. Wan, Y. Sun, X. Lu, and C. Zhao, "High precision angular measurement via dual imaging detectors," IEEE Sens. J. **19**, 7308–7312 (2019).
24. H. Yu, X. Jia, Q. Wan, C. Zhao, and Y. Sun, "High-resolution angular measurement arithmetic based on pixel interpolations," Measurement **149**, 106948 (2020).
25. H. Yu, Q. Wan, C. Zhao, L. Liang, and Y. Du, "High-resolution subdivision arithmetic and error analyses of photographic encoder," Acta Opt. Sin. **37**, 0312001 (2017).